Atmos. Chem. Phys., 24, 11943–11954, 2024
https://doi.org/10.5194/acp-24-11943-2024

Atmospheric Chemistry and Physics
Open Access
EGU

Research article

Formation of reactive nitrogen species promoted by iron ions through the photochemistry of a neonicotinoid insecticide

Zhu Ran[1,2], Yanan Hu[1,2,3], Yuanzhe Li[1,2], Xiaoya Gao[1,2], Can Ye[4], Shuai Li[5], Xiao Lu[5], Yongming Luo[1,2,3], Sasho Gligorovski[6,7,8], and Jiangping Liu[1,2]

[1]Faculty of Environmental Science and Engineering, Kunming University of Science and Technology, Kunming 650500, China
[2]The Innovation Team for Volatile Organic Compounds Pollutants Control and Resource Utilization of Yunnan Province, The Higher Educational Key Laboratory for Odorous Volatile Organic Compounds Pollutants Control of Yunnan Province, Kunming 650500, China
[3]Faculty of Chemical Engineering, Kunming University of Science and Technology, Kunming 650500, China
[4]Faculty of Environmental Science and Engineering, Peking University, Beijing 100871, China
[5]School of Atmospheric Sciences, Sun Yat-sen University, Southern Marine Science and Engineering Guangdong Laboratory (Zhuhai), Zhuhai, Guangdong 519082, China
[6]State Key Laboratory of Organic Geochemistry and Guangdong Provincial Key Laboratory of Environmental Protection and Resources Utilization, Guangzhou Institute of Geochemistry, Chinese Academy of Sciences, Guangzhou 510640, China
[7]Guangdong-Hong Kong-Macao Joint Laboratory for Environmental Pollution and Control, Guangzhou Institute of Geochemistry, Chinese Academy of Science, Guangzhou 510640, China
[8]Chinese Academy of Science, Center for Excellence in Deep Earth Science, Guangzhou 510640, China

Correspondence: Yanan Hu (huyanan0917@163.com), Sasho Gligorovski (gligorovski@gig.ac.cn), and Jiangping Liu (liujiangping18@mails.ucas.ac.cn)

Received: 12 April 2024 – Discussion started: 17 April 2024
Revised: 7 July 2024 – Accepted: 12 August 2024 – Published: 28 October 2024

Abstract. Nitrous acid (HONO) and nitrogen oxides ($NO_x = NO + NO_2$) are important atmospheric pollutants and key intermediates in the global nitrogen cycle, but their sources and formation mechanisms are still poorly understood. Here, we investigated the effect of soluble iron (Fe^{3+}) on the photochemical behavior of a widely used neonicotinoid (NN) insecticide, nitenpyram (NPM), in the aqueous phase. The yields of HONO and NO_x increased significantly when NPM solution was irradiated in the presence of iron ions (Fe^{3+}). We propose that the enhanced HONO and NO_2 emissions from the photodegradation of NPM in the presence of iron ions result from the redox cycle between Fe^{3+} and Fe^{2+} and the generated reactive oxygen species (ROS) by electron transfer between the excited triplet state of NPM and molecular oxygen (O_2). Using the laboratory-derived parameterization based on kinetic data and gridded downward solar radiation, we estimate that the photochemistry of NPM induced by Fe^{3+} releases 0.50 and 0.77 Tg N yr^{-1} of NO_x and HONO, respectively, into the atmosphere.

This study suggests a novel source of HONO and NO_x during daytime and potentially helps to narrow the gap between field observations and model outcomes of HONO in the atmosphere. The suggested photochemistry of NPM can be an important contribution to the global nitrogen cycle affecting the atmospheric oxidizing capacity and climate change.

Published by Copernicus Publications on behalf of the European Geosciences Union.

1 Introduction

Neonicotinoids (NNs) are a class of systemic insecticides that have been widely used in agriculture and horticulture since the 1990s (Bass et al., 2015), accounting for one-third of the total world insecticide market (Simon-Delso et al., 2015) and experiencing growing use in recent decades (Botías et al., 2015; Morrissey et al., 2015). They are highly water-soluble and persistent in the environment and can be transported to surface waters via runoff, leaching, or spray drift. NNs have been detected in various aquatic ecosystems, such as rivers, lakes, wetlands, and coastal waters, at concentrations ranging from 12.45 ng L^{-1} to 225 µg L^{-1} (Pan et al., 2020; Anderson et al., 2013). Increasing public perception of NN insecticide pollution has led to significant research efforts devoted to revealing the effect of insecticide application on humans (Cimino et al., 2017; Han et al., 2017), birds (Hallmann et al., 2014; Millot et al., 2017), animals (Morrissey et al., 2015; Gibbons et al., 2015), and pollinators (especially bees) (Kessler et al., 2015; Raine and Gill, 2015; Goulson et al., 2015). In the environment, NN insecticides can undergo various chemical processes, photolysis being one of their major fates (Lu et al., 2015; González-Mariño et al., 2018). Recent studies have focused mainly on the photochemistry of NN insecticides and their related atmospheric lifetimes and quantum yields (Lu et al., 2015; González-Mariño et al., 2018; Aregahegn et al., 2017, 2018). It has been shown that the ozonolysis of NN insecticides on various surfaces could contribute to the formation of gaseous nitrous acid (HONO) (W. Wang et al., 2020). Gaseous nitrous oxide (N_2O), which is a potent greenhouse gas, was previously identified as the gas-phase product in the photolysis of solid thin films of NNs (nitenpyram, acetamiprid, thiamethoxam, thiacloprid, clothianidin, and dinotefuran), with yields of $\Delta N_2O/\Delta NN > 0.5$ in air at both 313 and 254 nm (Wang et al., 2019; Aregahegn et al., 2017, 2018). Palma et al. (2020) used a gas-flow reactor connected to a NO_x analyzer, and the production of gaseous NO/NO_2 began during irradiation (300–450 nm) of imidacloprid. However, the crucial role of NN insecticides in the global nitrogen cycle at the air–water interface is largely unknown.

Nitenpyram (NPM) is one of the most commonly used NN insecticides. It represents a systemic NN insecticide which is widely distributed among soils, dust particles, and the aqueous environment (Botías et al., 2015; Ezell et al., 2019). Once released into the environment, NPM will be transformed into other products by absorbing sunlight ($\lambda > 290$ nm) and/or reacting with atmospheric oxidants such as the hydroxyl radical (OH) and ozone (O_3) (W. Wang et al., 2020). NPM is a nitroalkene, which is structurally similar to nitroaromatic compounds (Ar-NO_2). Previous studies have indicated that photolysis of Ar-NO_2 can be a source of HONO and NO_x in the atmosphere (Fukuhara et al., 2001; Yang et al., 2021; Bejan et al., 2006). HONO represents one of the main sources of OH radicals in the urban atmosphere, contributing up to 80 % of the total OH production (Alicke et al., 2003; Young et al., 2012; Zheng et al., 2020). The main identified HONO sources in urban air are photolysis of nitrates (Ye et al., 2017; Gen et al., 2021) and light-induced heterogeneous reaction of NO_2 with environmental surfaces (Liu et al., 2019, 2020, 2023; Monge et al., 2010; Han et al., 2016). However, there is a discrepancy between the modeled HONO values and field observations of HONO during the daytime, suggesting that there are missing HONO sources in the atmosphere. Meanwhile, the quantification of NO_x is also of great significance for the atmospheric cycle of nitrogen species, as NO_x plays a crucial role in photochemical smog and acid rain formation. Therefore, it is worthwhile exploring the contribution of NPM photolysis to HONO and NO_x, which in turn can offer guidance for the development of more sustainable next-generation insecticide products.

Iron species are ubiquitous on Earth surfaces, including water, soil, and the air–water interface (Gen et al., 2021). A recent study (Kebede et al., 2016) showed that one of the less explored HONO sources could be highly dependent on the photochemical reaction of iron. The photosensitivity, oxidation state, and catalytic properties of iron could enable it to possibly react with NN insecticide compounds that are enriched at the air–water interface. Previous studies on the mechanism of NN oxidation in the ferric aqueous phase have focused on the photo-Fenton reaction (Malato et al., 2001; Lacson et al., 2018; Wang et al., 2022; Nguyen et al., 2020; Sedaghat et al., 2016) and heterogeneous-phase photocatalysis (Rózsa et al., 2019; Sun and Liu, 2019; Hayat et al., 2019; Soltani-nezhad et al., 2019). As reported recently, the photolysis of iron can generate several reactive oxygen species (ROS), e.g., $O_2^{\bullet-}/HO_2^{\bullet}$, which can trigger the redox cycle between Fe^{3+} and Fe^{2+} (Gen et al., 2021) and promote NN insecticide oxidation. Meanwhile, iron ions inhibit the degradation of organic matter through the formation of complexes, which is mainly due to fluorescence bursting. This complexation may cause inhibition of the excited singlet state and thus photoformation of the triplet excited state (Wan et al., 2019). In addition to the NN insecticides and iron photosensitizers, nitrate (NO_3^-) and nitrite (NO_2^-) can absorb sunlight in the actinic region and initiate production of ROS (Vione and Scozzaro, 2019). Moreover, reaction between Fe^{2+} and NO_3^- may be a potentially important source of HONO (Gen et al., 2021). To this end, we suggest that photolysis of NPM in the presence of iron may contribute to a missing atmospheric HONO source.

To the best of our knowledge, this is the first investigation to measure the photochemical production of HONO and NO_x from NPM photolysis in the absence and presence of soluble iron. The photolysis frequency of HONO ($J_{NPM\rightarrow HONO}$), NO_2 ($J_{NPM\rightarrow NO_2}$), and NO ($J_{NPM\rightarrow NO}$) during the NPM reaction at the air–water interface was investigated. The kinetics and mechanism of HONO and NO_x formation in the presence of soluble iron were evaluated. This study highlights an overlooked source of HONO and NO_x from NN-covered wa-

ter surfaces that may play a critical role in the atmospheric nitrogen cycle and the evaluation of the atmospheric oxidation capacity.

2 Experiments

2.1 Material and sample preparation

Solid NPM (Aladdin, China) was dissolved in ultra-pure water to prepare an aqueous NPM solution (0.5 mg mL^{-1}) before each experiment. $FeCl_3$ (98 %; Aladdin, China) was used as the source of different concentrations of aqueous Fe^{3+} (0.1–0.8 mg mL^{-1}), and their solutions were prepared by dissolving the corresponding mass of $FeCl_3$ in ultra-pure water.

2.2 Experimental setup

The circular reactor consisted of a double layer of quartz glass (3.4 cm height, 7.5 cm inner diameter) connected to a thermostatic bath (XOSC-20, China), which allowed operation at a constant temperature of 298 K (Fig. S1 in the Supplement). The previously prepared sample solution was placed in the circular reactor and exposed to a xenon lamp (Perfect Light, PLS-SXE 300, China) vertically above the reactor. The xenon lamp was 12 cm away from the liquid level of NPM. The spectral irradiance of the xenon lamp was measured using a calibrated spectroradiometer (HP 350 UVP, China) (Fig. S1). Dry air collected from an air generator (HY-3, China) was used for the experiment. During the whole experiment, a constant flow of 800 mL min^{-1} of dry air was controlled using an electronic soap film flowmeter (SCal Plus, China). The UV absorption spectra of the NPM aqueous solutions in the absence or presence of iron ions were measured using the UV–Vis double-beam spectrophotometer (Shimadzu 2600, Japan) (Fig. S2 and Test S1).

2.3 NO_x, HONO, NPM, and ROS measurements

NO, NO_2, and HONO were detected using a chemiluminescence NO_x analyzer (42i, THERMO) with a molybdenum converter. NO was measured by reacting NO with O_3 to produce characteristic luminescence, and the intensity of the luminescence was proportional to the concentration of NO. In the detection of NO_2, a molybdenum catalyst was used to convert NO_2 to NO. A quartz tube (25 cm length, 2.9 cm inner diameter) filled with a certain amount of crystalline (Na_2CO_3) was introduced to capture HONO between the circular reactor outlet and the NO_x analyzer. It is well known that almost all HONO molecules can contact Na_2CO_3 when using molybdenum converters, achieving a high capture efficiency of HONO. Therefore, HONO can be quantified indirectly by the difference between the NO_2 signal and the Na_2CO_3 tube (Monge et al., 2010; Cazoir et al., 2014; Brigante et al., 2008; Zhou et al., 2018). The quantification of NPM before and after the reaction was determined using high-performance liquid chromatography (HPLC). The mobile phase was a mixture of water and acetonitrile with a flow rate of 0.5 mL min^{-1} at 80 : 20 (v/v). The column temperature was kept at 30 °C, the injection volume was 20 µL, and the detection wavelength was set to 270 nm. The external standard method was used for the quantitative determination of NPM. Photoproductions of O_2-•, $^1O_2$, and OH were quantified using 5,5-Dimethyl-1-Pyrroline-N-oxide (DMPO), 2,2,6,6-Tetramethylpiperidine (TEMP) and 5,5-Dimethyl-1-Pyrroline-N-oxide (DMPO), respectively, as the chemical probe molecules.

2.4 Kinetic analysis

The NPM photolysis kinetics were described using a first-order reaction (Eq. 1), and the half-life ($t_{1/2}$) was calculated using Eq. (2):

$$C_t = C_0 \times e^{-kt}, \quad (1)$$

$$t_{1/2} = \ln(2)/k, \quad (2)$$

where C_0 (mg mL^{-1}) is the initial concentration of NPM, C_t (mg mL^{-1}) is the NPM concentration at time t, and k is the first-order rate constant.

2.5 The photolysis frequency

The photolysis frequencies of NPM to HONO and NO_x were calculated using Eqs. (3) and (4), respectively:

$$J_{\mathrm{NPM}\rightarrow\mathrm{HONO}} = \frac{Q M_{\mathrm{NPM}} \int_0^t C_t^{\mathrm{HONO}} \mathrm{d}t}{60 \times 10^{-3} N_{\mathrm{A}} \times t \times (m_0 + m_t)/2}, \quad (3)$$

$$J_{\mathrm{NPM}\rightarrow\mathrm{NO}_x} = \frac{Q M_{\mathrm{NPM}} \int_0^t C_t^{\mathrm{NO}_x} \mathrm{d}t}{60 \times 10^{-3} N_{\mathrm{A}} \times t \times (m_0 + m_t)/2}, \quad (4)$$

where Q (mL min^{-1}) and M_{NPM} (g mol^{-1}) are the total gas flow rates in the reactor and the molar mass of NPM, respectively; t (min) is the irradiation time; $C_t^{\mathrm{NO}_x}$ (molec. cm^{-3}) is the concentration of gaseous HONO or NO_x formed by photolysis of NPM during the irradiation period; N_{A} is the Avogadro number; and M_0 (mg) and M_t (mg) are the masses at the beginning and end of the NPM photolysis experiments.

2.6 Flux densities of HONO and NO_x

The flux densities of HONO and NO_x were estimated using the following equations:

$$\mathrm{HONO}_{\mathrm{flux}} = \frac{[\mathrm{HONO}] \cdot V}{s \cdot t}, \quad (5)$$

$$\mathrm{NO}_{x\,\mathrm{flux}} = \frac{[\mathrm{NO}_x] \cdot V}{s \cdot t}, \quad (6)$$

where HONO flux is expressed (molec. cm^{-2} s^{-1}), [HONO] is the concentration of HONO (molec. cm^{-3}), V (cm^3) is the

volume of the reactor, S (cm^2) is the surface of the reactor, and t (s) is the residence time of HONO in the circular reactor.

2.7 Global simulation of NO_x and HONO fluxes

We estimated the global inventory of the NO_x and HONO fluxes produced by NPM photochemistry using the observation-constrained parameterization scheme and hourly solar radiation data. Gridded and hourly downward solar radiation data are obtained from Modern-Era Retrospective analysis for Research and Application Version 2 (MERRA-2)-assimilated meteorological fields. We calculated the flux of NO_x and HONO for each model grid at a horizontal resolution of $0.5° \times 0.625°$ (consistent with the MERRA-2 radiation dataset) following Eqs. (S1)–(S3) in the Supplement but assuming that the environmental NPM concentration is 3 orders of magnitude smaller than the experimental condition of $0.5\,mg\,L^{-1}$. The parameterization of HONO and NO_x productions from NPM photolysis at the Fe^{3+} concentration of $0.025\,mg\,L^{-1}$ used in our estimation is based on Eqs. (S1)–(S3), and more details can be seen in Test S2.

3 Results and discussion

3.1 Absorbance of NPM in the presence of Fe^{3+}

Figure S1 shows the absorbance of NPM ($0.05\,mg\,mL^{-1}$) in the dilute aqueous phase and at different Fe^{3+} concentrations, adjusted by $FeCl_3$, along with the emission spectrum of the solar simulator and the sunlight. The presence of Fe^{3+} at various initial concentrations slightly enhanced the absorbance of NPM, especially at a high Fe^{3+} concentration ($0.08\,mg\,mL^{-1}$), indicating that no Fe^{3+}–NPM complexes were generated (Liu et al., 2022). Indeed, pH is a sensitive parameter that can significantly affect the light-absorbing properties and degree of photochemical degradation of organic compounds (Cai et al., 2018; Zhou et al., 2019). The interaction between Fe^{3+} and organics as well as possible aggregation of organics at low pH may also influence the light absorption at low wavelengths (Weishaar et al., 2003). The change in Fe^{3+} concentrations may alter the pH of the system, which in turn may affect the protonation or deprotonation degree of NPM and therefore its absorption spectrum (Zhou et al., 2019). The pH value of the NPM solution in the presence of Fe^{3+} varies between 2.4 and 3.4, and under this pH condition NPM ($pKa = 3.1$) exists in both ionic and neutral forms (Hậu et al., 2021; Bonmatin et al., 2014).

3.2 Kinetic analysis

Iron ions are ubiquitous in natural waters, with concentrations ranging from 10^{-7} to 10^{-4} M and even higher in contaminated waters (Li et al., 2018; Faust and Hoigné, 1990). Previous studies have shown that iron ions play an important role in the photolysis of pesticides and may affect the photodegradation of organic pollutants (Faust and Hoigné, 1990; Zhao et al., 2014). The photolysis kinetics of NPM were performed to account for the loss of NPM. The photolysis of NPM at different concentrations of Fe^{3+} obeyed pseudo-first-order kinetics (Fig. 1), with half-lives ranging from 135.1 to 223.6 min as the Fe^{3+} concentration increased from 0 to $0.8\,mg\,mL^{-1}$ (Table S1 in the Supplement).

The light-induced degradation of NPM was significantly inhibited at low Fe^{3+} concentrations ($C_{(Fe^{3+})} < 0.5\,mg\,mL^{-1}$; Fig. 1 and Table S1). In contrast, when the concentration of Fe^{3+} reaches $0.8\,mg\,mL^{-1}$, the degradation of NPM is promoted (Fig. 1), exhibiting a rate constant of $0.00513\,min^{-1}$ (Table S1). Previous studies have demonstrated that the degradation of organic compounds in the presence of Fe^{3+} is dose-dependent (Lin et al., 2019; Deguillaume et al., 2005). For instance, Fe^{3+} slightly inhibits the photodegradation of fluazaindolizine at concentrations of 1–5 $mg\,L^{-1}$ but promotes its degradation rate at concentrations ranging between 0.1 and $0.5\,mg\,L^{-1}$ (Lin et al., 2019). Deguillaume et al. (2005) reported that photodegradation of flupyradifurone, a novel neonicotinoid pesticide, was faster at lower Fe^{3+} concentrations and slowed down with the increase in Fe^{3+} concentrations.

The main reason for the inhibition effect of Fe^{3+} is the attenuation of radiation due to the absorption by Fe^{3+} (light screening), which reduces the light absorbance by NPM and its photodegradation. At the same time, it has been extensively confirmed that $[Fe^{3+}(OH)]^{2+}$ is the main form of Fe^{3+} and exhibits great photoactivity in aqueous solution at $pH = 3$ (Bai et al., 2023; Li et al., 2023). In the presence of $[Fe^{3+}(OH)]^{2+}$, strong oxidizing ROS are produced, which promote hydroxylation and degradation of NPM (Andrianirinaharivelo et al., 1995; Mazellier et al., 1997). As a result, at $pH = 3$, the photodegradation of NPM is accelerated at high Fe^{3+} concentrations.

In this study, a high Fe^{3+} concentration ($0.8\,mg\,mL^{-1}$) promoted the photodegradation of NPM and the formation of HONO and NO_x (see the section below). The enhanced formation of HONO and NO_x can be ascribed to ROS, as described in Sect. 3.5.

3.3 HONO and NO_x formations by NPM photolysis

The experiments of NPM photodegradation in the aqueous phase were performed to measure the HONO and NO_x production in the presence of different Fe^{3+} concentrations. The HONO and NO_x production by spontaneous reaction of NPM in the dark was negligible (Fig. S3 in the Supplement). When the NPM samples were exposed to light irradiation, the concentrations of HONO and NO_x quickly increased (Fig. 2a).

Only the concentration of NO formed upon irradiation of NPM is almost the same in the absence of Fe^{3+} and in the presence of $0.25\,mg\,mL^{-1}$ of Fe^{3+} (Fig. 2a). In the

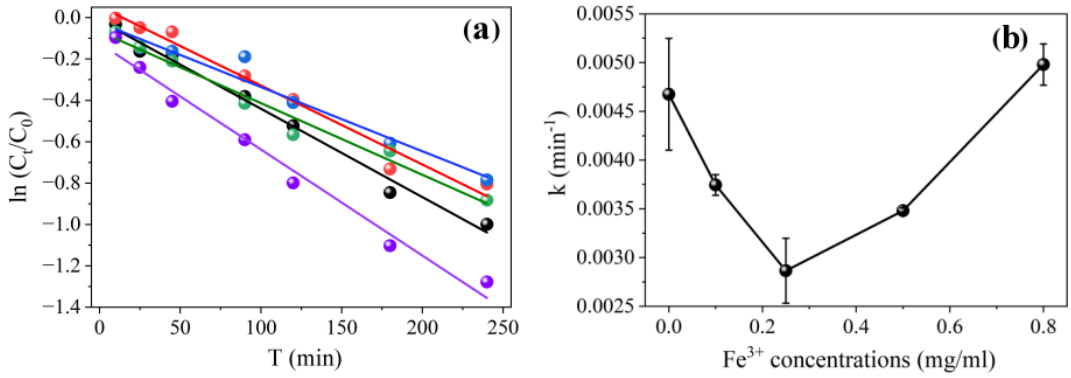

Figure 1. **(a)** The kinetics of NPM (0.5 mg mL^{-1}) in the absence of Fe^{3+} (dark line) and in the presence of different Fe^{3+} concentrations: 0.1 mg mL^{-1} (red line), 0.25 mg mL^{-1} (blue line), 0.5 mg mL^{-1} (green line), and 0.8 mg mL^{-1} (purple line). **(b)** The rate constants of NPM light-induced degradation (0.5 mg mL^{-1}) at different Fe^{3+} concentrations.

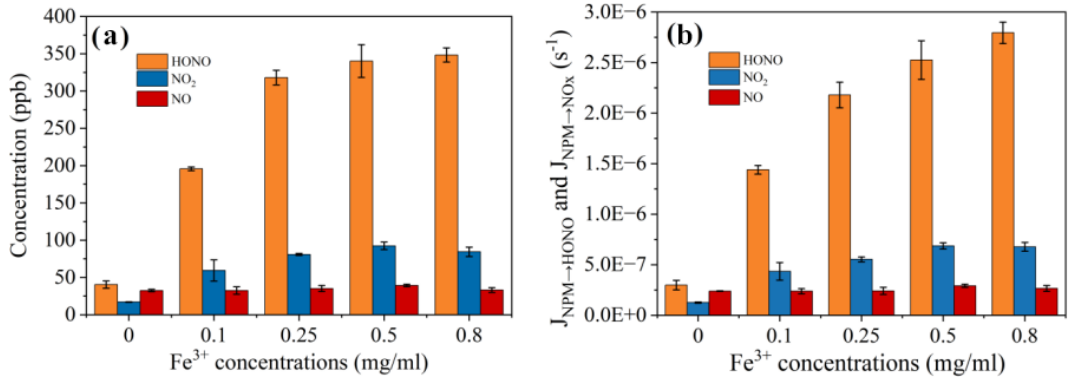

Figure 2. **(a)** Concentrations of NO, NO_2, and HONO produced by NPM photolysis at different concentrations of Fe^{3+}. **(b)** $J_{NPM\rightarrow HONO}$ and $J_{NPM\rightarrow NO_x}$ from NPM at different concentrations of Fe^{3+} and an irradiation intensity of 169.4 W m^{-2} at $300 < \lambda < 400$ nm, $T = 298$ K.

meantime, the NO_2 formation increased significantly with the increase in Fe^{3+} concentrations and remained almost steady during the whole light exposure time (Fig. S3). Moreover, when the experiments were shifted to high concentrations of soluble iron (0.25–0.8 mg mL^{-1}), significantly enhanced NO_2 and NO formation was observed that then slowly decreased with the light exposure time. In order to better understand the effect of iron on HONO and NO_x production, the quantities of HONO and NO_x were compared when the NPM photolysis reached a relatively stable stage (120 min). It is important to note that the formed HONO (341 ppb) was significantly higher at an iron concentration of 0.8 mg mL^{-1} compared to the HONO (37 ppb) that formed in the absence of iron. Similarly, the quantity of the formed NO_2 increased from 17 ppb in the absence of iron to 96 ppb in the presence of 0.5 mg mL^{-1} of Fe^{3+}. However, further increases in the iron concentration to 0.8 mg mL^{-1} tended to decrease the production of NO_2. Figure 2 shows that the NO concentrations remained almost unchanged with the increase in the iron concentration. To quantify the photolysis quantum yields of HONO, NO_2, and NO formation from NPM photolysis, we estimated the photolysis frequency of HONO ($J_{NPM\rightarrow HONO}$), NO_2 ($J_{NPM\rightarrow NO_2}$), and NO ($J_{NPM\rightarrow NO}$) formation, respectively (Fig. 2b). $J_{NPM\rightarrow HONO}$ varied from $(2.99 \pm 0.46) \times 10^{-7}$ s^{-1} in the absence of Fe^{3+} to $(2.79 \pm 0.10) \times 10^{-6}$ s^{-1} in the presence of 0.8 mg mL^{-1} Fe^{3+}. Simultaneously, $J_{NPM\rightarrow NO_2}$ increased ca. 5-fold from $(1.25 \pm 0.06) \times 10^{-7}$ s^{-1} in the absence of Fe^{3+} to $(6.77 \pm 0.44) \times 10^{-7}$ s^{-1} at 0.8 mg mL^{-1} of Fe^{3+}. Regarding $J_{NPM\rightarrow NO}$, there were nearly no discernible changes observed, with values ranging from $(2.38 \pm 0.27) \times 10^{-7}$ to $(2.92 \pm 0.15) \times 10^{-7}$ s^{-1}. A previous study (Yang et al., 2021) found that the photolysis frequency of HONO and NO in nitrophenol solid-phase films (4-nitrophenol, 4-nitrocatechol, 3,5-dinitrosalicylic acid, 3-nitrosalicylic acid, and 5-nitrosalicylic acid) varied in the ranges $(0.34–4.16) \times 10^{-7}$ and $(0.38–3.21) \times 10^{-7}$ s^{-1}, respectively, when irradiated by xenon lamps. NPM liquid-phase photolysis produced HONO and NO_x at a photolysis frequency of 10^{-7}, but the addition of iron resulted in a photolysis frequency of 10^{-6} for HONO, suggesting that iron significantly facilitated the release of HONO. In order to

compare the efficiency of NPM at different Fe^{3+} concentrations in producing HONO and NO, Φ_{HONO} and Φ_{NO_x} were displayed (Table S2 in the Supplement). It can be concluded that NPM with high Fe^{3+} concentrations had more important HONO formations as compared to pure NPM.

3.4 HONO and NO_x surface flux densities

Figure 3 summarizes the results obtained in terms of HONO formation rates per unit of exposed surface area, flux densities of HONO, NO_2, and NO.

The flux density values of HONO and NO_x indicate that direct photolysis dominated the transformation process of the NPM samples in the absence of Fe^{3+}. However, the introduction of soluble iron leads to significantly increased HONO and NO_2 yields during the first 10 min of the reaction time. Further progress of the reaction up to 2 h leads to slightly increased flux densities of NO_2 and HONO. In contrast, the NO formation showed a slow decrease after the addition of Fe^{3+}. A recent study (Aregahegn et al., 2017) demonstrated that photolysis of a solid film consisting of imidacloprid (IMD) did not lead to HONO and NO_x formation and that N_2O was rather the main gas-phase product. However, it is important to note that the introduction of Fe^{3+} promotes the photodegradation of NPM to produce more HONO and NO_x. In the section below we suggest a tentative reaction mechanism to describe the formation of HONO and NO_2 upon irradiation of NPM at the water surface in the presence of soluble iron.

3.5 Mechanism describing the formation of HONO and NO_x

We speculate that, in the presence of Fe^{3+}, the decrease in dissolved nitrogen species that resulted from the photodegradation of NPM is the reason for the formation of HONO and NO_x. Therefore, ROS and dissolved nitrogen-containing ions were measured upon photodegradation of NPM in the presence of Fe^{3+}. The generation of superoxide radicals (O_2-•), singlet oxygen ($^1O_2$), and hydroxyl radicals (OH) was quantified using DMPO, TEMP, and DMPO, respectively, as the chemical probe molecules. Figure 4a shows that, in the absence of Fe^{3+}, the photodegradation of NPM induces generation of OH, O_2-•, and $^1O_2$, which can be ascribed to the electron transfer between the excited triplet state of NPM and the molecular oxygen (O_2) (Segura et al., 2008; Mostafa and Rosario-Ortiz, 2013; Marin et al., 2012; Wang et al., 2021).

It has been reported that, under UV light irradiation, Fe^{3+} photoreduction regenerates Fe^{2+}, accelerating the process due to the formation of new OH radicals (Segura et al., 2008). The electron paramagnetic resonance (EPR) measurements revealed an interesting phenomenon where the increase in the Fe^{3+} concentration promotes the consumption rate of ROS (Fig. 4b) rather than the production rate. The generated ROS would react with lower-valence nitrogen-containing species to form HONO and NO_x. Based on this finding, we suggest a tentative reaction mechanism which could explain the formation of large quantities of HONO and NO_x during the photochemical degradation of NPM. The photochemical generation of ROS could be driven by two pathways. Pathway I is the excited triplet state of NPM ($^3NPM^*$) that can be formed under light irradiation (Reaction R1) (Mora Garcia et al., 2021), and then, by reacting with water molecules (Reaction R2), it can trigger the formation of ROS such as OH radicals, accompanied by the generation of O_2-• through the transformation between radical anions of NPM (NPM-•) and dissolved oxygen (Reaction R3) (Wang et al., 2021). Furthermore, with the progress of the photodegradation of NPM, an increase in O_2-• and OH formation was observed (Fig. 4a), favoring HONO and NO_2 formation (Reactions R6–R8). In the presence of Fe^{3+}, formation of OH radicals by Reaction (R4) occurs as well (Mazellier et al., 1997). In addition, nitrate ions (NO_3^-) and nitrite ions (NO_2^-) in the aqueous phase are formed by Reactions (R5)–(R7). Peroxynitrate ($OONO_2^-$) is formed by reaction of O_2-• with NO_2, which thermally decomposes to form NO_2^- and O_2, which further leads to HONO formation (Reaction R6) (X. Wang et al., 2020; Lammel et al., 2002; Goldstein et al., 1998). The reaction between O_2-• and NO can lead to the formation of NO_2^- and NO_3^-, with a relatively fast rate constant of $4.3 \times 10^9\ M^{-1}\ s^{-1}$ (Goldstein and Czapski, 1995) producing a peroxynitrite ($OONO^-$) which then yields NO_3^- through internal rearrangement (Reaction R7) (Loegager and Sehested, 1993). At neutral pH (pKa = 6.5), the OONOH product can also be formed by protonation, which can coexist with $OONO^-$ to form NO_2^- (Reaction R7) (Guptaet et al., 2009). Previous studies have shown that the reaction between OH and NO_2^- will generate NO_2 (Reaction R8) (Loegager and Sehested,, 1993), and a sharp increase in the HONO concentration occurs immediately from reaction between NO_2^- and H^+ (Reaction R9), which is expected to be an important pathway of HONO formation.

At low Fe^{3+} concentrations (0.25–0.5 mg mL^{-1}), the degradation rate of NPM was completely inhibited, which was not the case for higher Fe^{3+} concentrations (0.5–0.8 mg mL^{-1}) (Fig. 1). Notably, Fe^{3+} plays an important role in providing an acidic environment (pH = 2.4–3.4) in the reaction system, which is followed by the redox reaction between Fe^{2+} and NO_3^- to produce NO_2 and consequently increase the amount of NO_2 (Reaction R10) (Fig. S3). It has been shown that NO_3^- undergoes a photochemical process and thus produces HONO (Reaction R11) and NO_2 (Reaction R12) (Ye et al., 2016; Zhou et al., 2011).

$$NPM \xrightarrow{h\nu} {}^3NPM^* \quad \text{(R1)}$$

$$^3NPM^* + H_2O \rightarrow H^+ + \cdot OH + NPM^{-\bullet} \quad \text{(R2)}$$

$$NPM^{-\bullet} + O_2 \rightarrow NPM + O_2^{-\bullet} \quad \text{(R3)}$$

$$Fe^{3+} + H_2O \xrightarrow{h\nu} Fe^{2+} + \cdot OH + H^+ \quad \text{(R4)}$$

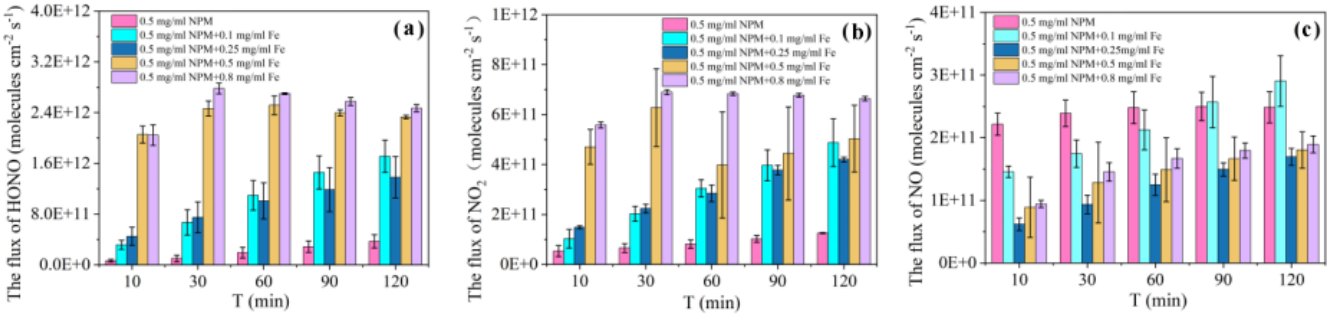

Figure 3. Flux densities of HONO **(a)**, NO_2 **(b)**, and NO **(c)** determined as a function of the photolysis time of NPM in the presence of different concentrations of Fe^{3+}.

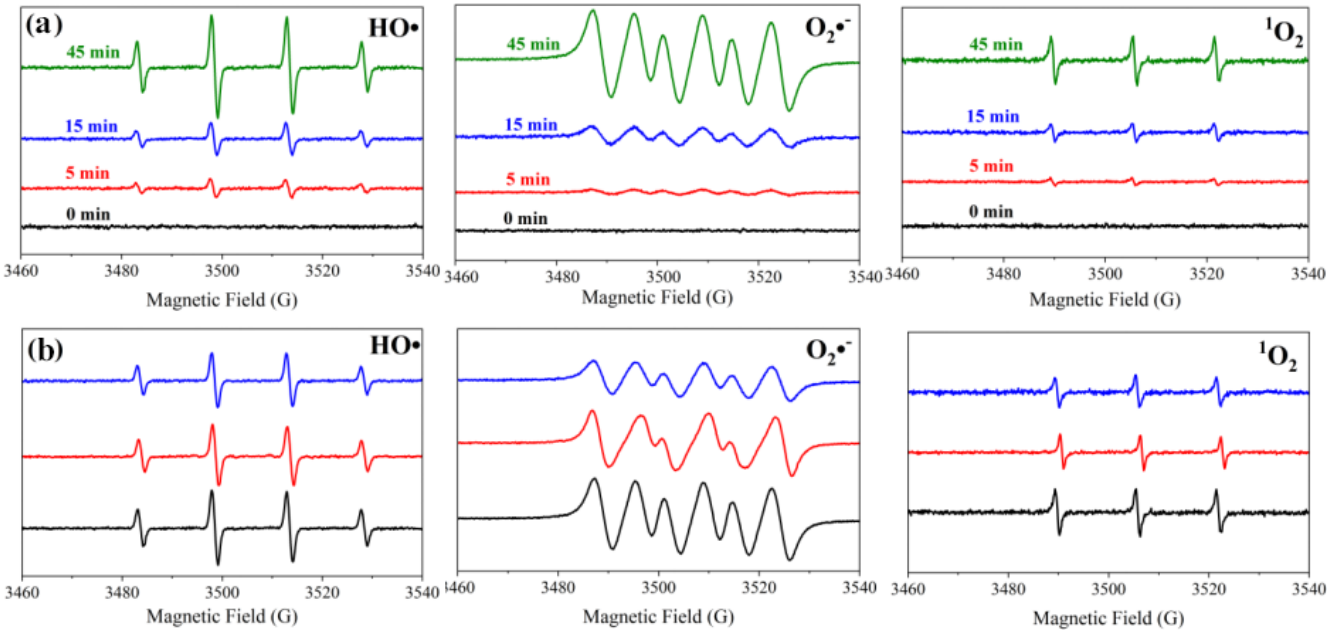

Figure 4. **(a)** EPR spectra obtained upon photodegradation of NPM (0.5 mg mL^{-1}) in the absence of Fe^{3+} as a function of the reaction time. **(b)** EPR spectra obtained upon 45 min photodegradation of NPM (0.5 mg mL^{-1}) in the absence of Fe^{3+} (dark line) and in the presence of 0.25 mg mL^{-1} of Fe^{3+} (red line) and 0.8 mg mL^{-1} of Fe^{3+} (blue line).

$$2NO_2 + H_2O \rightarrow HNO_2 + HNO_3 \quad \text{(R5)}$$

$$O_2^{-\bullet} + NO_2 \rightarrow OONO_2^- \rightarrow O_2 + NO_2^- \xrightarrow{+H^+\ (pKa=3.2)} HONO \quad \text{(R6)}$$

$$O_2^{-\bullet} + NO \rightarrow OONO^-\ (NO_3^-) \leftrightharpoons OONOH \xrightarrow{+OONO^-} O_2 + 2NO_2^- + H^+ \xrightarrow{pKa=3.2} HONO \quad \text{(R7)}$$

$$NO_2^- + {\bullet}OH \rightarrow NO_2 + OH^- \quad \text{(R8)}$$

$$NO_2^- + H^+ \xrightarrow{pKa=3.2} HONO \quad \text{(R9)}$$

$$Fe^{2+} + NO_3^- + 2H^+ \rightarrow Fe^{3+} + NO_2(g) + H_2O \quad \text{(R10)}$$

$$NO_3^- \xrightarrow{h\nu} [NO_3^-]^* \rightarrow O(^3P) + NO_2^- \xrightarrow{H^+} HONO \quad \text{(R11)}$$

$$NO_3^- \xrightarrow{h\nu} [NO_3^-]^* \xrightarrow{H^+} NO_2 + {\bullet}OH \quad \text{(R12)}$$

A simplified illustration of the reaction mechanism is shown in Fig. S4 in the Supplement. As shown in Fig. S3, the HONO and NO_2 production during the photodegradation of NPM in the presence of Fe^{3+} is significantly enhanced relative to that in the absence of iron ions. High Fe^{3+} concentrations (0.5–0.8 mg mL^{-1}) promote HONO and NO_2 formation compared to low Fe^{3+} concentrations (0.25–0.5 mg mL^{-1}). The formed NO_3^- and NO_2^- were also measured by ion chromatography analysis to evaluate the effect of Fe^{3+} (see the details in Test S1 and Fig. S5 in the Supplement). As shown in Fig. S5, the concentrations of NO_3^- and NO_2^- decreased sharply in the presence of Fe^{3+} compared to those in the absence of Fe^{3+}. These results suggest that HONO and NO_2 enhancement during the irradiation of NPM solutions containing Fe^{3+} can be ascribed to the transformation of the product distribution from NO_3^- and NO_2^-

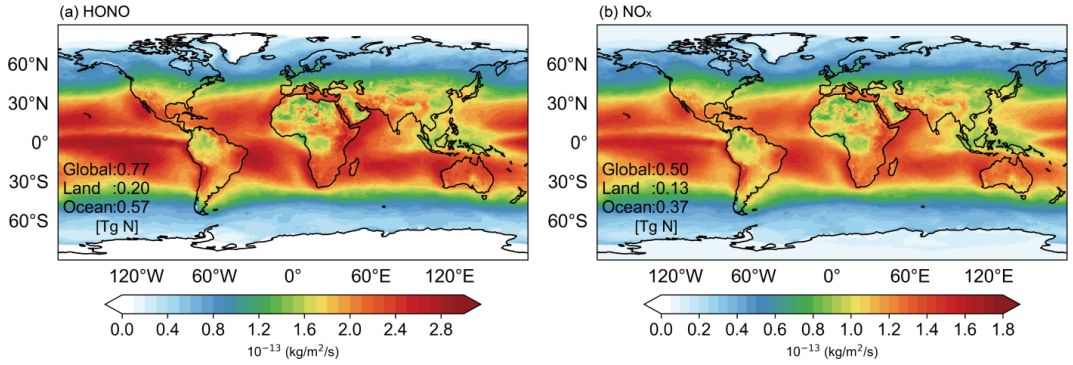

Figure 5. Global emissions of HONO **(a)** and NO_x **(b)**, produced by photochemistry of NPM in the presence of iron ions for the year 2017.

rather than a change in the product formation from the photodegradation of NPM.

4 Conclusions and outlook

Laboratory study revealed the formation of a greenhouse gas (N_2O) through photolysis of NPM (Aregahegn et al., 2018), but previously the theoretical calculation had predicted that photolysis of NNs would generate NO_2 (Palma et al., 2020).

The current study reveals that the light-induced degradation of NPM leads to enhanced production of HONO and NO_x driven by secondary photochemistry between redox reaction of Fe^{3+}/Fe^{2+} and photoproduced ROS. We quantified the photochemical HONO and NO_x formation through NPM photodegradation, and we suggest that this chemistry may represent a significant source of HONO and NO_x in regions where surface waters are polluted with NN insecticides.

In order to estimate the relative importance of the NPM photolysis to global HONO and NO_x emissions in the atmosphere, we parameterized the global HONO and NO_x production related to NPM photochemistry, based on the NPM photolysis kinetic data and gridded downward solar radiation. The parameterization of HONO and NO_x production from NPM photolysis at the Fe^{3+} concentration of $0.025\,mg\,L^{-1}$ used in our estimation is based on Eqs. (S1)–(S3). The concentrations of NNs vary from several nanogram per liter to hundreds of microgram per liter (Anderson et al., 2013). In view of the high concentration of NPM ($50\,000\,\mu g\,L^{-1}$) used in our experiments, we selected a rationalization parameter scheme related to the environmental concentration of NPM ($50\,\mu g\,L^{-1}$). The kinetic data have shown that the rate constant (k) is faster at low NPM concentrations compared to that of high NPM concentrations (Fig. S6 in the Supplement). Current chemical models do not explicitly consider this source of reactive nitrogen species. In this way, we are able to generate an hourly dataset of the NO_x and HONO fluxes released from NPM chemistry, and we analyze the amounts and spatial patterns of the fluxes in Fig. 5. We note that, although such estimation is rather simplified and can be biased in terms of the spatial heterogeneity as we do not consider the spatial variation of environmental NPM concentrations, our study represents a pioneering attempt to quantify the global source of HONO and NO_x from the NPM photochemistry, as current chemical models do not explicitly consider this source of reactive nitrogen species. This inventory can then be applied in chemical models to quantify the environmental impact of HONO and NO_x fluxes emerging from NPM photochemistry. Details about the parameterization of HONO and NO_x production that emerged from NPM photochemistry are given in Text S2 in the Supplement. Figure 5 shows the spatial distributions of HONO and NO_x fluxes produced by NPM photochemistry in the tested year of 2017. The results indicate that the globally produced HONO and NO_x fluxes based on NPM photochemistry are 0.77 and $0.5\,Tg\,N\,yr^{-1}$, respectively, making a total of $1.27\,Tg\,N\,yr^{-1}$.

The total production of HONO and NO_x emissions due to NPM photochemistry ($1.27\,Tg\,N\,yr^{-1}$) represents 3.5 % of the anthropogenic emissions of NO_x related to fossil fuel in the year 2017 ($36.2\,Tg\,N\,yr^{-1}$, from the Community Emissions Data System (CEDS) inventory) and about 14.8 % of the soil emissions ($8.6\,Tg\,N\,yr^{-1}$, Lu et al., 2021). The highest HONO and NO_x fluxes (74 %) are produced by the photochemistry of NPM at the ocean surface in the presence of iron ions, especially tropical oceans. The latter can be ascribed to the higher solar radiation in the tropical regions. As displayed in Fig. S7 in the Supplement, it is obvious to see that the spatial distribution of solar radiation is particularly strong in tropical oceanic regions, which can further confirm the higher HONO and NO_x fluxes at the ocean surface. The high reactive nitrogen emissions could also appear over other water surfaces like inland waters and lakes worldwide through similar mechanisms induced by NPM photochemistry. Further studies are needed to quantify the relative importance of the recognized HONO and NO_x sources from NPM photochemistry on a global scale as well as the impact on tropospheric ozone and OH in the marine boundary layer.

Data availability. All raw data can be provided by the corresponding authors upon request.

Supplement. The Supplement contains 10 additional figures, three tables, and text. The supplement related to this article is available online at: https://doi.org/10.5194/acp-24-11943-2024-supplement.

Author contributions. JL and SG designed the research. ZR, YuL, and YH performed the laboratory experiments. JL, ZR, XG, SL, CY, XL, and SG analyzed and interpreted the data from the laboratory experiments. YH and YoL contributed to the relevant discussion on the manuscript. JL, YH, and SG wrote the paper. All the authors discussed the results and commented on the manuscript.

Competing interests. The contact author has declared that none of the authors has any competing interests.

Disclaimer. Publisher's note: Copernicus Publications remains neutral with regard to jurisdictional claims made in the text, published maps, institutional affiliations, or any other geographical representation in this paper. While Copernicus Publications makes every effort to include appropriate place names, the final responsibility lies with the authors.

Acknowledgements. We would like to thank our reviewers and editor for their constructive suggestions, which improved the quality of this paper.

Financial support. This research has been supported by the National Natural Science Foundation of China (grant nos. 42207127, 42030712, 42177087, 41977187, and 4221101064) and the Applied Basic Research Foundation of Yunnan Province (grant nos. 202301AT070424, 202101BE070001-027, 202101BG070084, and 202302AG050002). The Yunnan Revitalization Talents Support Plan's Young Talent Project and the High-End Foreign Experts Project financed this research.

Review statement. This paper was edited by Markus Ammann and reviewed by two anonymous referees.

References

Alicke, B., Geyer, A., Hofzumahaus, A., Holland, F., Konrad, S., Pätz, H. W., Schäfer, J., Stutz, J., Volz-Thomas, A., and Platt, U.: OH formation by HONO photolysis during the BERLIOZ experiment, J. Geophys. Res.-Atmos., 108, 8247, https://doi.org/10.1029/2001jd000579, 2003.

Anderson, T. A., Salice, C. J., Erickson, R. A., McMurry, S. T., Cox, S. B., and Smith, L. M.: Effects of landuse and precipitation on pesticides and water quality in playa lakes of the southern high plains, Chemosphere, 92, 84–90, https://doi.org/10.1016/j.chemosphere.2013.02.054, 2013.

Andrianirinaharivelo, S., Mailhot, G., and Bolte, M.: Photodegradation of organic pollutants induced by complexation with transition metals (Fe^{3+} and Cu^{2+}) present in natural waters, Sol. Energ. Mat. Sol. C., 38, 459–474, https://doi.org/10.1016/0927-0248(94)00238-x, 1995.

Aregahegn, K. Z., Shemesh, D., Gerber, R. B., and Finlayson-Pitts, B. J.: Photochemistry of Thin Solid Films of the Neonicotinoid Imidacloprid on Surfaces, Environ. Sci. Technol., 51, 2660–2668, https://doi.org/10.1021/acs.est.6b04842, 2017.

Aregahegn, K. Z., Ezell, M. J., and Finlayson-Pitts, B. J.: Photochemistry of Solid Films of the Neonicotinoid Nitenpyram, Environ. Sci. Technol., 52, 2760–2767, https://doi.org/10.1021/acs.est.7b06011, 2018.

Bai, X., Yang, Q., Guo, Y., Hao, B., Zhang, R., Duan, R., and Li, J.: Alkyl halide formation from degradation of carboxylic acids in the presence of Fe(III) and halides under light irradiation, Water. Res., 235, 119842, https://doi.org/10.1016/j.watres.2023.119842, 2023.

Bass, C., Denholm, I., Williamson, M. S., and Nauen, R.: The global status of insect resistance to neonicotinoid insecticides, Pestic. Biochem. Phys., 121, 78–87, https://doi.org/10.1016/j.pestbp.2015.04.004, 2015.

Bejan, I., Abd El Aal, Y., Barnes, I., Benter, T., Bohn, B., Wiesen, P., and Kleffmann, J. R.: The photolysis of ortho-nitrophenols: a new gas phase source of HONO, Phys. Chem. Chem. Phys., 8, 2028–2035, https://doi.org/10.1039/b516590c, 2006.

Bonmatin, J. M., Giorio, C., Girolami, V., Goulson, D., Kreutzweiser, D. P., Krupke, C., Liess, M., Long, E., Marzaro, M., Mitchell, E. A. D., Noome, D. A., Simon-Delso, N., and Tapparo, A.: Environmental fate and exposure; neonicotinoids and fipronil, Environ. Sci. Pollut. R., 22, 35–67, https://doi.org/10.1007/s11356-014-3332-7, 2014.

Botías, C., David, A., Horwood, J., Abdul-Sada, A., Nicholls, E., Hill, E., and Goulson, D.: Neonicotinoid Residues in Wildflowers, a Potential Route of Chronic Exposure for Bees, Environ. Sci. Technol., 49, 12731–12740, https://doi.org/10.1021/acs.est.5b03459, 2015.

Brigante, M., Cazoir, D., D'Anna, B., George, C., and Donaldson, D. J.: Photoenhanced Uptake of NO_2 by Pyrene Solid Films, J. Phys. Chem. A, 112, 9503–9508, https://doi.org/10.1021/jp802324g, 2008.

Cai, J., Zhi, G., Yu, Z., Nie, P., Gligorovski, S., Zhang, Y., Zhu, L., Guo, X., Li, P., He, T., He, Y., Sun, J., and Zhang, Y.: Spectral changes induced by pH variation of aqueous extracts derived from biomass burning aerosols: Under dark and in presence of simulated sunlight irradiation, Atmos. Environ., 185, 1–6, https://doi.org/10.1016/j.atmosenv.2018.04.037, 2018.

Cazoir, D., Brigante, M., Ammar, R., D'Anna, B., and George, C.: Heterogeneous photochemistry of gaseous NO_2 on solid fluoranthene films: A source of gaseous nitrous acid (HONO) in the urban environment, J. Photoch. Photobio. A, 273, 23–28, https://doi.org/10.1016/j.jphotochem.2013.07.016, 2014.

Cimino, A. M., Boyles, A. L., Thayer, K. A., and Perry, M. J.: Effects of Neonicotinoid Pesticide Exposure on Human Health: A Systematic Review, Environ. Health Persp., 125, 155–162, https://doi.org/10.1289/ehp515, 2017.

Deguillaume, L., Leriche, M., Desboeufs, K., Mailhot, G., George, C., and Chaumerliac, N.: Transition Metals in Atmospheric Liq-

uid Phases: Sources, Reactivity, and Sensitive Parameters, Chem. Rev., 105, 3388–3431, https://doi.org/10.1021/cr040649c, 2005.

Ezell, M. J., Wang, W., Shemesh, D., Ni, A., Gerber, R. B., and Finlayson-Pitts, B. J.: Experimental and Theoretical Studies of the Environmental Sensitivity of the Absorption Spectra and Photochemistry of Nitenpyram and Analogs, ACS Earth Space Chem., 3, 2063–2075, https://doi.org/10.1021/acsearthspacechem.9b00179, 2019.

Faust, B. C. and Hoigné, J.: Photolysis of Fe(III)-hydroxy complexes as sources of OH radicals in clouds, fog and rain, Atmos. Environ. A-Gen., 24, 79–89, https://doi.org/10.1016/0960-1686(90)90443-q, 1990.

Fukuhara, K., Kurihara, M., and Miyata, N.: Photochemical Generation of Nitric Oxide from 6-Nitrobenzo[a]pyrene, J. Am. Chem. Soc., 123, 8662–8666, https://doi.org/10.1021/ja0109038, 2001.

Gen, M., Zhang, R., and Chan, C. K.: Nitrite/Nitrous Acid Generation from the Reaction of Nitrate and Fe(II) Promoted by Photolysis of Iron–Organic Complexes, Environ. Sci. Technol., 55, 15715–15723, https://doi.org/10.1021/acs.est.1c05641, 2021.

Gibbons, D., Morrissey, C., and Mineau, P.: A review of the direct and indirect effects of neonicotinoids and fipronil on vertebrate wildlife, Environ. Sci. Pollut. R., 22, 103–118, https://doi.org/10.1007/s11356-014-3180-5, 2015.

Goldstein, S. and Czapski, G.: The reaction of NO• with $O_2^{\bullet-}$ and $HO_2^{\bullet-}$: A pulse radiolysis study, Free Radical Bio. Med., 19, 505–510, https://doi.org/10.1016/0891-5849(95)00034-u, 1995.

Goldstein, S., Czapski, G., Lind, J., and Merenyi, G.: Mechanism of Decomposition of Peroxynitric Ion (O_2NOO^-): Evidence for the Formation of $O_2^{\bullet-}$ and $^{\bullet}NO_2$ Radicals, Inorg. Chem., 37, 3943–3947, https://doi.org/10.1021/ic9800511, 1998.

González-Mariño, I., Rodríguez, I., Rojo, L., and Cela, R.: Photodegradation of nitenpyram under UV and solar radiation: Kinetics, transformation products identification and toxicity prediction, Sci. Total Environ., 644, 995–1005, https://doi.org/10.1016/j.scitotenv.2018.06.318, 2018.

Goulson, D., Nicholls, E., Botías, C., and Rotheray, E. L.: Bee declines driven by combined stress from parasites, pesticides, and lack of flowers, Science, 347, 1255957, https://doi.org/10.1126/science.1255957, 2015.

Gupta, D., Harish, B., Kissner, R., and Koppenol, W. H.: Peroxynitrate is formed rapidly during decomposition of peroxynitrite at neutral pH, Dalton T., 29, 5730–5736, https://doi.org/10.1039/b905535e, 2009.

Hallmann, C. A., Foppen, R. P. B., van Turnhout, C. A. M., de Kroon, H., and Jongejans, E.: Declines in insectivorous birds are associated with high neonicotinoid concentrations, Nature, 511, 341–343, https://doi.org/10.1038/nature13531, 2014.

Han, C., Yang, W., Wu, Q., Yang, H., and Xue, X.: Heterogeneous Photochemical Conversion of NO_2 to HONO on the Humic Acid Surface under Simulated Sunlight, Environ. Sci. Technol., 50, 5017–5023, https://doi.org/10.1021/acs.est.5b05101, 2016.

Han, W., Tian, Y., and Shen, X.: Human exposure to neonicotinoid insecticides and the evaluation of their potential toxicity: An overview, Chemosphere, 192, 59–65, https://doi.org/10.1016/j.chemosphere.2017.10.149, 2017.

Hậu, N. C., Đào, Đ. T. H., and Đào, L. T. A.: Simultaneous Determination of Neonicotinoid Pesticides in Tea-Tree Plantation Soil by Ultra-Performance Liquid Chromatography Tandem Mass Spectrometry, Tạp chí Khoa học., 18, 403–413, 2021.

Hayat, W., Zhang, Y. Q., Hussain, I., Du, X. D., Du, M. M., Yao, C. H., Huang, S. B., and Si, F.: Efficient degradation of imidacloprid in water through iron activated sodium persulfate, Chem. Eng. J., 370, 1169–1180, https://doi.org/10.1016/j.cej.2019.03.261, 2019.

Kebede, M. A., Bish, D. L., Losovyj, Y., Engelhard, M. H., and Raff, J. D.: The Role of Iron-Bearing Minerals in NO_2 to HONO Conversion on Soil Surfaces, Environ. Sci. Technol., 50, 8649–8660, https://doi.org/10.1021/acs.est.6b01915, 2016.

Kessler, S. C., Tiedeken, E. J., Simcock, K. L., Derveau, S., Mitchell, J., Softley, S., Radcliffe, A., Stout, J. C., and Wright, G. A.: Bees prefer foods containing neonicotinoid pesticides, Nature, 521, 74–76, https://doi.org/10.1038/nature14414, 2015.

Lacson, C. F. Z., de Luna, M. D. G., Dong, C. D., Garcia-Segura, S., and Lu, M. C.: Fluidized-bed Fenton treatment of imidacloprid: Optimization and degradation pathway, Sustainable Environ. Res., 28, 309–314, https://doi.org/10.1016/j.serj.2018.09.001, 2018.

Lammel, G., Perner, D., and Warneck, P.: Decomposition of pernitric acid in aqueous solution, J. Phys. Chem., 94, 6141–6144, https://doi.org/10.1021/j100378a091, 2002.

Li, C., Zhang, D., Peng, J., and Li, X.: The effect of pH, nitrate, iron (III) and bicarbonate on photodegradation of oxytetracycline in aqueous solution, J. Photoch. Photobio. A, 356, 239–247, https://doi.org/10.1016/j.jphotochem.2018.01.004, 2018.

Li, P., Gemayel, R., Li, X., Liu, J., Tang, M., Wang, X., Yang, Y., Al-Abadleh, H. A., and Gligorovski, S.: Formation of nitrogen-containing gas phase products from the heterogeneous (photo)reaction of NO_2 with gallic acid, Commun. Chem., 6, 198, https://doi.org/10.1038/s42004-023-01003-3, 2023.

Lin, H., Pang, K., Ma, Y., and Hu, J.: Photodegradation of fluazaindolizine in water under simulated sunlight irradiation: Identification of transformation products and elucidation of transformation mechanism, Chemosphere, 214, 543–552, https://doi.org/10.1016/j.chemosphere.2018.09.151, 2019.

Liu, H., Zhang, Z., Tu, Y.-N., Li, Y., Lei, Y., and Tian, S.: Dual roles of Cu^{2+} complexation with dissolved organic matter on the photodegradation of trace organic pollutants: Triplet- and OH-induced reactions, Sci. Total Environ., 815, 152934, https://doi.org/10.1016/j.scitotenv.2022.152934, 2022.

Liu, J., Li, S., Mekic, M., Jiang, H., Zhou, W., Loisel, G., Song, W., Wang, X., and Gligorovski, S.: Photoenhanced Uptake of NO_2 and HONO Formation on Real Urban Grime, Environ. Sci. Tech. Let., 6, 413–417, https://doi.org/10.1021/acs.estlett.9b00308, 2019.

Liu, J., Deng, H., Li, S., Jiang, H., Mekic, M., Zhou, W., Wang, Y., Loisel, G., Wang, X., and Gligorovski, S.: Light-Enhanced Heterogeneous Conversion of NO_2 to HONO on Solid Films Consisting of Fluorene and Fluorene/Na_2SO_4: An Impact on Urban and Indoor Atmosphere, Environ. Sci. Technol., 54, 11079–11086, https://doi.org/10.1021/acs.est.0c02627, 2020.

Liu, J., Li, B., Deng, H., Yang, Y., Song, W., Wang, X., Luo, Y., Francisco, J. S., Li, L., and Gligorovski, S.: Resolving the Formation Mechanism of HONO via Ammonia-Promoted Photosensitized Conversion of Monomeric NO_2 on Urban Glass Surfaces, J. Am. Chem. Soc., 145, 11488–11493, https://doi.org/10.1021/jacs.3c02067, 2023.

Loegager, T. and Sehested, K.: Formation and decay of peroxynitric acid: a pulse radiolysis study, Phys. Chem., 97, 10047–10052, https://doi.org/10.1021/j100141a025, 1993.

Lu, X., Ye, X., Zhou, M., Zhao, Y., Weng, H., Kong, H., Li, K., Gao, M., Zheng, B., Lin, J., Zhou, F., Zhang, Q., Wu, D., Zhang, L., and Zhang, Y.: The underappreciated role of agricultural soil nitrogen oxide emissions in ozone pollution regulation in North China, Nat. Commun., 12, 5021, https://doi.org/10.1038/s41467-021-25147-9, 2021.

Lu, Z., Challis, J. K., and Wong, C. S.: Quantum Yields for Direct Photolysis of Neonicotinoid Insecticides in Water: Implications for Exposure to Nontarget Aquatic Organisms, Environ. Sci. Tech. Let., 2, 188–192, https://doi.org/10.1021/acs.estlett.5b00136, 2015.

Malato, S., Caceres, J., Agüera, A., Mezcua, M., Hernando, D., Vial, J., and Fernández-Alba, A. R.: Degradation of imidacloprid in water by photo-fenton and TiO_2 photocatalysis at a solar pilot plant:: A comparative study, Environ. Sci. Technol., 35, 4359–4366, https://doi.org/10.1021/es000289k, 2001.

Marin, M. L., Santos-Juanes, L., Arques, A., Amat, A. M., and Miranda, M. A.: Organic Photocatalysts for the Oxidation of Pollutants and Model Compounds, Chem. Rev., 112, 1710–1750, https://doi.org/10.1021/cr2000543, 2012.

Mazellier, P., Jirkovsky, J., and Bolte, M.: Degradation of Diuron Photoinduced by Iron(III) in Aqueous Solution, Pestic. Sci., 49, 259–267, https://doi.org/10.1002/(sici)1096-9063(199703)49:3<259::Aid-ps526>3.0.Co;2-h, 1997.

Millot, F., Decors, A., Mastain, O., Quintaine, T., Berny, P., Vey, D., Lasseur, R., and Bro, E.: Field evidence of bird poisonings by imidacloprid-treated seeds: a review of incidents reported by the French SAGIR network from 1995 to 2014, Environ. Sci. Pollut. R., 24, 5469–5485, https://doi.org/10.1007/s11356-016-8272-y, 2017.

Monge, M. E., D'Anna, B., Mazri, L., Giroir-Fendler, A., Ammann, M., Donaldson, D. J., and George, C.: Light changes the atmospheric reactivity of soot, P. Natl. Acad. Sci. USA, 107, 6605–6609, https://doi.org/10.1073/pnas.0908341107, 2010.

Mora Garcia, S. L., Pandit, S., Navea, J. G., and Grassian, V. H.: Nitrous Acid (HONO) Formation from the Irradiation of Aqueous Nitrate Solutions in the Presence of Marine Chromophoric Dissolved Organic Matter: Comparison to Other Organic Photosensitizers, ACS Earth Space Chem., 5, 3056–3064, https://doi.org/10.1021/acsearthspacechem.1c00292, 2021.

Morrissey, C. A., Mineau, P., Devries, J. H., Sanchez-Bayo, F., Liess, M., Cavallaro, M. C., and Liber, K.: Neonicotinoid contamination of global surface waters and associated risk to aquatic invertebrates: A review, Environ. Int., 74, 291–303, https://doi.org/10.1016/j.envint.2014.10.024, 2015.

Mostafa, S. and Rosario-Ortiz, F. L.: Singlet Oxygen Formation from Wastewater Organic Matter, Environ. Sci. Technol., 47, 8179–8186, https://doi.org/10.1021/es401814s, 2013.

Nguyen, D. D. D., Huynh, K. A., Nguyen, X. H., and Nguyen, T. P.: Imidacloprid degradation by electro-Fenton process using composite Fe_3O_4–Mn_3O_4 nanoparticle catalyst, Res. Chem. Intermediat., 46, 4823–4840, https://doi.org/10.1007/s11164-020-04246-0, 2020.

Palma, D., Arbid, Y., Sleiman, M., de Sainte-Claire, P., and Richard, C.: New Route to Toxic Nitro and Nitroso Products upon Irradiation of Micropollutant Mixtures Containing Imidacloprid: Role of NO_x and Effect of Natural Organic Matter, Environ. Sci. Technol., 54, 3325–3333, https://doi.org/10.1021/acs.est.9b07304, 2020.

Pan, X., Wang, Z., Chen, C., Li, H., Li, X., Zhang, Q., Wang, X., and Zhang, Y.: Research on the distribution of neonicotinoid and fipronil pollution in the Yangtze River by high-performance liquid chromatography, Anal. Methods-UK, 12, 5581–5590, https://doi.org/10.1039/d0ay01558j, 2020.

Raine, N. E. and Gill, R. J.: Tasteless pesticides affect bees in the field, Nature, 521, 38–39, https://doi.org/10.1038/nature14391, 2015.

Rózsa, G., Náfrádi, M., Alapi, T., Schrantz, K., Szabó, L., Wojnárovits, L., Takács, E., and Tungler, A.: Photocatalytic, photolytic and radiolytic elimination of imidacloprid from aqueous solution: Reaction mechanism, efficiency and economic considerations, Appl. Catal. B-Environ., 250, 429–439, https://doi.org/10.1016/j.apcatb.2019.01.065, 2019.

Sedaghat, M., Vahid, B., Aber, S., Rasoulifard, M. H., Khataee, A., and Daneshvar, N.: Electrochemical and photo-assisted electrochemical treatment of the pesticide imidacloprid in aqueous solution by the Fenton process: effect of operational parameters, Res. Chem. Intermediat., 42, 855–868, https://doi.org/10.1007/s11164-015-2059-5, 2016.

Segura, C., Zaror, C., Mansilla, H. D., and Mondaca, M. A.: Imidacloprid oxidation by photo-Fenton reaction, J. Hazard. Mater., 150, 679–686, https://doi.org/10.1016/j.jhazmat.2007.05.018, 2008.

Simon-Delso, N., Amaral-Rogers, V., Belzunces, L. P., Bonmatin, J. M., Chagnon, M., Downs, C., Furlan, L., Gibbons, D. W., Giorio, C., Girolami, V., Goulson, D., Kreutzweiser, D. P., Krupke, C. H., Liess, M., Long, E., McField, M., Mineau, P., Mitchell, E. A. D., Morrissey, C. A., Noome, D. A., Pisa, L., Settele, J., Stark, J. D., Tapparo, A., Van Dyck, H., Van Praagh, J., Van der Sluijs, J. P., Whitehorn, P. R., and Wiemers, M.: Systemic insecticides (neonicotinoids and fipronil): trends, uses, mode of action and metabolites, Environ. Sci. Pollut. R., 22, 5–34, https://doi.org/10.1007/s11356-014-3470-y, 2015.

Soltani-nezhad, F., Saljooqi, A., Shamspur, T., and Mostafavi, A.: Photocatalytic degradation of imidacloprid using GO/FeO/TiO-NiO under visible radiation: Optimization by response level method, Polyhedron, 165, 188–196, https://doi.org/10.1016/j.poly.2019.02.012, 2019.

Sun, Y. H. and Liu, X.: Efficient visible-light photocatalytic degradation of imidacloprid and acetamiprid using a modified carbon nitride/tungstophosphoric acid composite induced by a nucleophilic addition reaction, Appl. Surf. Sci., 485, 423–431, https://doi.org/10.1016/j.apsusc.2019.04.203, 2019.

Vione, D. and Scozzaro, A.: Photochemistry of Surface Fresh Waters in the Framework of Climate Change, Environ. Sci. Technol., 53, 7945–7963, https://doi.org/10.1021/acs.est.9b00968, 2019.

Wan, D., Sharma, V. K., Liu, L., Zuo, Y. G., and Chen, Y.: Mechanistic Insight into the Effect of Metal Ions on Photogeneration of Reactive Species from Dissolved Organic Matter, Environ. Sci. Technol., 53, 5778–5786, https://doi.org/10.1021/acs.est.9b00538, 2019.

Wang, W., Ezell, M. J., Lakey, P. S. J., Aregahegn, K. Z., Shiraiwa, M., and Finlayson-Pitts, B. J.: Unexpected formation of oxygen-free products and nitrous acid from the ozonolysis of the

neonicotinoid nitenpyram, P. Natl. Acad. Sci. USA, 117, 11321–11327, https://doi.org/10.1073/pnas.2002397117, 2020.

Wang, W. C., Huang, D. Y., Wang, D. X., Tan, M. X., Geng, M. Y., Zhu, C. Y., Chen, N., and Zhou, D. M.: Extensive production of hydroxyl radicals during oxygenation of anoxic paddy soils: Implications to imidacloprid degradation, Chemosphere, 286, 131565, https://doi.org/10.1016/j.chemosphere.2021.131565, 2022.

Wang, W. H., Aregahegn, K. Z., Andersen, S. T., Ni, A. Z., Rohrbacher, A. F., Nielsen, O. J., and Finlayson-Pitts, B. J.: Quantum Yields and NO_2 Formation from Photolysis of Solid Films of Neonicotinoids, J. Agr. Food Chem., 67, 1638–1646, https://doi.org/10.1021/acs.jafc.8b05417, 2019.

Wang, X., Dalton, E. Z., Payne, Z. C., Perrier, S., Riva, M., Raff, J. D., and George, C.: Superoxide and Nitrous Acid Production from Nitrate Photolysis Is Enhanced by Dissolved Aliphatic Organic Matter, Environ. Sci. Tech. Let., 8, 53–58, https://doi.org/10.1021/acs.estlett.0c00806, 2020.

Wang, Y., Huang, D. D., Huang, W., Liu, B., Chen, Q., Huang, R., Gen, M., Mabato, B. R. G., Chan, C. K., Li, X., Hao, T., Tan, Y., Hoi, K. I., Mok, K. M., and Li, Y. J.: Enhanced Nitrite Production from the Aqueous Photolysis of Nitrate in the Presence of Vanillic Acid and Implications for the Roles of Light-Absorbing Organics, Environ. Sci. Technol., 55, 15694–15704, https://doi.org/10.1021/acs.est.1c04642, 2021.

Weishaar, J. L., Aiken, G. R., Bergamaschi, B. A., Fram, M. S., Fujii, R., and Mopper, K.: Evaluation of Specific Ultraviolet Absorbance as an Indicator of the Chemical Composition and Reactivity of Dissolved Organic Carbon, Environ. Sci. Technol., 37, 4702–4708, https://doi.org/10.1021/es030360x, 2003.

Yang, W., You, D., Li, C., Han, C., Tang, N., Yang, H., and Xue, X.: Photolysis of Nitroaromatic Compounds under Sunlight: A Possible Daytime Photochemical Source of Nitrous Acid?, Environ. Sci. Tech. Lett., 8, 747–752, https://doi.org/10.1021/acs.estlett.1c00614, 2021.

Ye, C., Gao, H., Zhang, N., and Zhou, X.: Photolysis of Nitric Acid and Nitrate on Natural and Artificial Surfaces, Environ. Sci. Technol., 50, 3530–3536, https://doi.org/10.1021/acs.est.5b05032, 2016.

Ye, C., Zhang, N., Gao, H., and Zhou, X.: Photolysis of Particulate Nitrate as a Source of HONO and NO_x, Environ. Sci. Technol., 51, 6849–6856, https://doi.org/10.1021/acs.est.7b00387, 2017.

Young, C. J., Washenfelder, R. A., Roberts, J. M., Mielke, L. H., Osthoff, H. D., Tsai, C., Pikelnaya, O., Stutz, J., Veres, P. R., Cochran, A. K., VandenBoer, T. C., Flynn, J., Grossberg, N., Haman, C. L., Lefer, B., Stark, H., Graus, M., de Gouw, J., Gilman, J. B., Kuster, W. C., and Brown, S. S.: Vertically Resolved Measurements of Nighttime Radical Reservoirs in Los Angeles and Their Contribution to the Urban Radical Budget, Environ. Sci. Technol., 46, 10965–10973, https://doi.org/10.1021/es302206a, 2012.

Zhao, Q., Zhao, H., Quan, X., Chen, S., and Zhang, Y.: Photochemical transformation of 2,2′,4,4′-tetrabromodiphenyl ether (BDE-47) in surface coastal waters: Effects of chloride and ferric ions, Mar. Pollut. Bull., 86, 76–83, https://doi.org/10.1016/j.marpolbul.2014.07.040, 2014.

Zheng, J., Shi, X., Ma, Y., Ren, X., Jabbour, H., Diao, Y., Wang, W., Ge, Y., Zhang, Y., and Zhu, W.: Contribution of nitrous acid to the atmospheric oxidation capacity in an industrial zone in the Yangtze River Delta region of China, Atmos. Chem. Phys., 20, 5457–5475, https://doi.org/10.5194/acp-20-5457-2020, 2020.

Zhou, S., Young, C. J., VandenBoer, T. C., Kowal, S. F., and Kahan, T. F.: Time-Resolved Measurements of Nitric Oxide, Nitrogen Dioxide, and Nitrous Acid in an Occupied New York Home, Environ. Sci. Technol., 52, 8355–8364, https://doi.org/10.1021/acs.est.8b01792, 2018.

Zhou, W., Mekic, M., Liu, J., Loisel, G., Jin, B., Vione, D., and Gligorovski, S.: Ionic strength effects on the photochemical degradation of acetosyringone in atmospheric deliquescent aerosol particles, Atmos. Environ., 198, 83–88, https://doi.org/10.1016/j.atmosenv.2018.10.047, 2019.

Zhou, X., Zhang, N., TerAvest, M., Tang, D., Hou, J., Bertman, S., Alaghmand, M., Shepson, P. B., Carroll, M. A., Griffith, S., Dusanter, S., and Stevens, P. S.: Nitric acid photolysis on forest canopy surface as a source for tropospheric nitrous acid, Nat. Geosci., 4, 440–443, https://doi.org/10.1038/ngeo1164, 2011.